Transactions on Energy Systems and Engineering Applications

Article

TS fuzzy control of PV assisted single phase three phase induction motor drive for rural pumping applications

Sareddy Venkata Rami Reddy [1], Rekha Mudundi[2], M. Kiran Kumar[3], Ch. Rami Reddy[4,8,*], T. Venkata Sai Kalyani[5], D. Ravi Kumar[6] and B. Nagi Reddy[7,*]

1 Department of Electrical and Electronics Engineering, JNTUA College of Engineering Pulivendula, Pulivendula - 516390, India
2 Department of Electrical and Electronics Engineering, Gokaraju Rangaraju Institute of Engineering and Technology, Hyderabad, Telangana-500090, India
3 Department of Electrical and Electronics Engineering, Koneru Lakshmaiah Education Foundation, Guntur - 522302, India
4 Department of Electrical and Electronics Engineering, Joginpally B R Engineering College, Hyderabad 500075, India
5 Department of Electrical and Electronics Engineering, Amrita Vishwa Vidyapeetham, Bangaluru-560035, India
6 Department of Electrical and Electronics Engineering, VNR Vignana Jyothi Institute of Engineering and Technology, Hyderabad, India
7 Department of Electrical and Electronics Engineering,Vignana Bharathi Institute of Technology, Hyderabad 501301, India
8 Applied Science Research Center, Applied Science Private University, Amman 11937, Jordan
* Correspondence: crreddy229@gmail.com, nagireddy208@gmail.com

Received: 12 July 2023; Accepted: 08 November 2023; Published: 30 April 2024

Abstract: The motor drives for aqua farms and large-scale irrigation system needs a reliable electric drive, which requires the continuous power supply and efficient control. However, the rural single phase power supply is frequently interrupted. Renewable assistance would improve the availability of supply and heuristic control approach improves robustness in control. This paper presents a three phase induction motor drive fed from single phase electric grid with assistance from PV and battery energy storage. TS-fuzzy based direct torque control is employed for robust control during load changes, and the topology, component modelling, front-end converter control, PV interface DC–DC converter control, and inverter control are presented. MATLAB/Simulink is used to simulate the proposed drive system. The performance of the proposed system is validated using simulation data for both steady-state and transient states.

How to cite this article: Sareddy Venkata Rami Reddy; Rekha Mudundi; M. Kiran Kumar; Ch. Rami Reddy; T. Venkata Sai Kalyani; D. Ravi Kumar; B. Nagi Reddy. TS fuzzy control of PV assisted single phase three phase induction motor drive for rural pumping applications. *Transactions on Energy Systems and Engineering Applications*, 5(1): 537, 2024. DOI:10.32397/tesea.vol5.n1.537

1. Introduction

Modern agricultural needs have spread electrical systems into pumping, spraying, tilling, ploughing, weed removal, reaping, irrigation, harvesting, aquaculture, and allied applications. The load requirements for these applications include control of torque or speed or a combination of torque and speed. Also, the power requirement is growing towards a few hundred kW for irrigation of huge farms and oxygenation of aqua farms [1]. In this context, three phase drives were found to be extended into high-power agricultural drives to meet high-power conversion requirements. Among the electrical drives three phase induction motor-based drives with voltage source inverters for variable speed control [2] are widely used for their ease of control, rugged construction, and ease of maintenance. In this context, several issues were to be dealt with the available single-phase supply to drive the three-phase motor [3, 4]. The three-phase drive when used with single phase supply would overheat capacitors [5]. This is because of increased ripple in capacitor. The diode in front-end converter had to draw increased current. This causes power dissipation more than rated value for which the heat sink was designed [6]. This deteriorates the reliability of the front-end converter with increased failure rate of converter switches and filter components [7, 8]. Also, the average power handling of the input terminals and converter components was raised. The identified choices to overcome such issues were either employing three phase drives having higher power rating or inclusion of additional components to share the current or ripple content in DC voltage [9].To smooth the DC output of the boost converter, which acts as input to the inverter, a Sliding Mode Controller (SMC) is implemented [10] for stabilizing the DC output of the boost converter. This stabilizing input voltage of the inverter can provide fewer harmonics to the motor, which can improve the lifetime of the motor as compared to high harmonics which improves the reliability [11, 12] and continuous availability of power supply of the drive. The problem of long-term interruptions in the power supply is addressed by integrating renewable energy sources (RES) with the DC-link [13, 14]. The Photovoltaic (PV) generation method, which converts free solar energy into usable electricity through the photovoltaic effect, is one of the most widely utilized RES. The PV systems can be categorized as standalone and grid connected [15, 16]. The applications that are related to Grid-connected are used to exchange energy with the utility grid and supply energy for local loads, as opposed to standalone PV systems, which can only offer electricity for distant loads that lack a source of power. The DC current from the PV module is transformed into alternating current in a solar PV system by an inverter that is connected to the grid [17]. After meeting the current demand, the PV system can transmit the excess energy to the grid when it is connected to it. Yet, excess energy is taken from the system when demand exceeds generation [18]. The output from the PV panel is stepped up using boost converter, which acts as an input to the inverter which is loaded with water pump through the three phase Induction Motor (IM) [19, 20]. A proper energy management system is required among all these sources to achieve cost effective system with best performance. The battery is used for responding in transient time periods. The proposed energy management system [21, 22] can reduce the consumption of diesel by operating it at maximum efficiency. Generally, submersible pumps are used in water pumping systems, and it seems the motor is underwater at high depth from the ground. This will create problems in sensing the speed of the motor. To avoid this issue, this paper implements a sensor-less speed controller. Speed estimation is very important in sensor less speed control, and it can be achieved by mathematical expressions [23]. However, speed estimation requires both input voltage and currents of IM. Hence, both voltage and current sensors are required.

To reduce ripples in torque, a direct torque controller (DTC) has been implemented for running the motor through the inverter. Further, to generate reference electromagnetic torque, a Takagi-Sugeno (TS) fuzzy-based controller [24] is incorporated with DTC [25, 26]. IFOC is simple and suitable for water pumping systems. As the advantages of sensorless control in submersible-based water pumping systems were stated, sensorless vector control is executed. The workflow of this paper, include the following steps:

1. Addressing the challenges involved in using a three-phase VFD fed by a single-phase source.
2. Highlighting the importance of reducing diesel consumption during power outages by converting from single-phase to three-phase supply.
3. Integrating a PV system with efficient energy management and battery backup to diminish the reliance on diesel fuel.
4. Employing Sliding Mode Control (SMC) to produce a smooth DC output for the inverter and utilizing a TS-Fuzzy based speed sensorless direct torque controller to minimize torque ripples.

The remaining article is organized in to various sections. Section 2 describes the system description, section 3 represents the control structure, section 4 presents the simulation results and section 5 presents the conclusions.

2. System description

The proposed drive for the water pumping application consists of a hybrid power supply from a single-phase grid, PV source, and battery bank. The system is designed for speed control of the three phase IM for varying pressure and head of water. Various components of the proposed drive were depicted in Fig. 1. The drive is designed to be operated at rural agricultural locations where only single-phase supply is available. The single-phase power supply at 230 V, 50 Hz, was considered for the study. The active front-end converter with few external components to make it controlled single phase ac to dc conversion [27]. The availability of sufficient space at rural agricultural farms to accommodate PV panels and associated conversion interface will aid in reliable and efficient operation. The optimal sizing algorithms determine the percentage of power share by the PV source. However, the maximum share is limited by the available space and the economics of the system. PV source that feed the DC bus is interfaced with it through a DC-DC converter to extract maximum power from the PV source corresponding to irradiance at any provided instance. Thus, PV source supplies its maximum power to the DC bus at the required voltage. The excess power from PV source if any could be utilized to charge the battery bank and supply it to the drive under unavailability of PV source as a backup source for short duration of time. However, the sizing and viability of battery backup is determined upon economics of the system [28]. The battery backup was considered in the study to achieve reliable operation of the drive under unavailability of grid power and PV power.

This consists of the bi-directional power converter for charging and discharging modes of the battery bank. The control includes the power supply at the DC bus voltage during discharging and the power supply to the battery bank at terminal voltage during charging operation. The DC bus of the drive is fed from three sources viz., single phase grid through active front end converter, PV source through MPPT enabled converter, and battery bank through the bi-directional power converter. A high capacitance value holds the average DC bus voltage stiff to feed the voltage source inverter. The VSI converts the available DC power at its input terminals into variable voltage and variable frequency AC power per load terminals' requirements [29]. The variable speed operation as demanded by the pump is delivered through the three-phase induction motor controlled by a voltage source inverter. Speed control is to be achieved at various torques owing to the lift of water from different depths and at varying pressures at different operating conditions. The controller's objectives include power conversion control at front-end conversion, MPP extraction control of the PV interface converter, and bi-directional power flow control at the battery bank interface. Apart from the power flow control at various drive components, it also has got the function of direct torque control of three phase IM through the VSI (see Fig. 8).

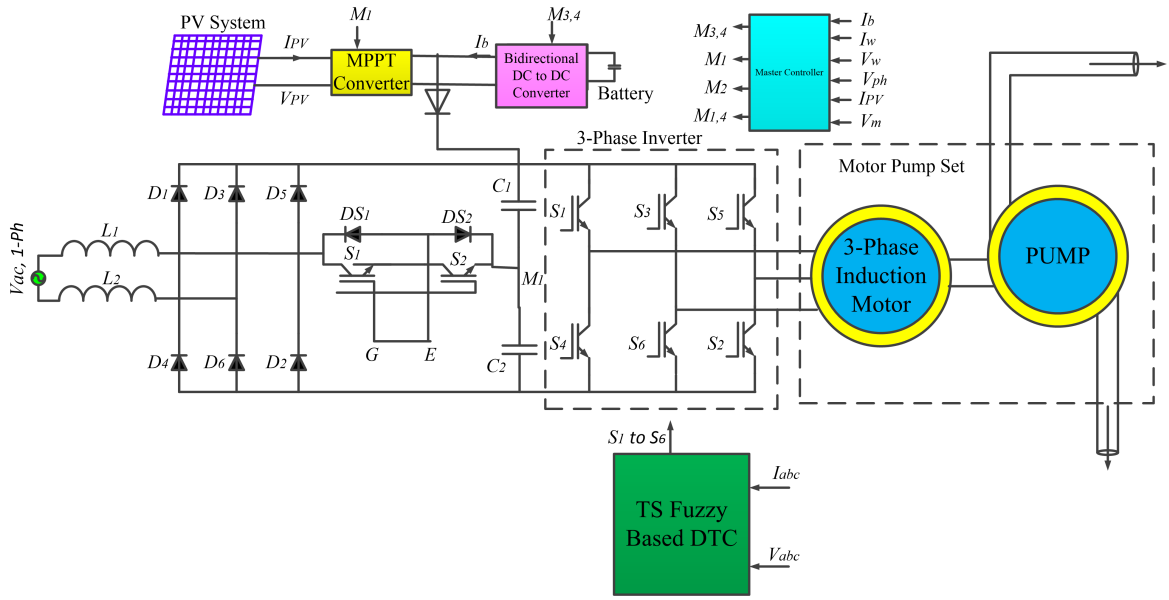

Figure 1. Single-phase to three-phase conversation to drive IM for the water pumping system.

2.1. Selection of Components

Generally, there is a static friction which is due to moving parts of the system. To overcome this breakaway torque T_b of motor/pump should be about 10–25 % of the nominal-torque. The pump starts supplying water only when the speed reaches a threshold value ωt. The rate of flow of water (Q, gal/min) linearly proportional with the speed of pump/motor ω, as expressed in equation (1) [3], and a nonlinear equation is presented in equation (2) that represents the water head and the necessary horsepower capacity of the motor is calculated using equation (3).

$$Q = \begin{cases} a\omega - b & \omega \geqslant \omega_t \\ 0 & \omega < \omega_t \end{cases} , \tag{1}$$

$$H = a_0\omega^2 + a_1\omega Q + a_2 Q^2 \ , \tag{2}$$

$$W_{hp} = Q \cdot H/3960 \ , \tag{3}$$

where a, a_0, a_1, a_2 and b are constants [28, 29] and W_{hp} is the horsepower, and H represents the total dynamic head (in feet).The pump should run at a power which is greater than W_{hp} to increase its efficiency. The brake horsepower (BHP) is the power essential at the pump shaft to pump an actual flow rate against a specified H, given by,

$$BHP = W_{hp}/(\text{pump} - \text{efficiency} \cdot \text{drive} - \text{efficiency}) \ . \tag{4}$$

The maximum speed and maximum power can be used to calculate the torque on the motor, i.e.,load torque as T_l=25 Nm. But, there will a linear increase in the load torque from T_b to T_l when the water flows from underground to round level. The water's weight will rise on the engine (i.e., the quantity of water from the pump to the outlet or ground point). This seems that the load torque will be very low at starting and will increase like a ramp while the water is coming out to the ground level. Generally, there is static friction due to moving parts of the system. To overcome this, 10-25% of the nominal torque should be considered as the motor breakaway torque T_b.

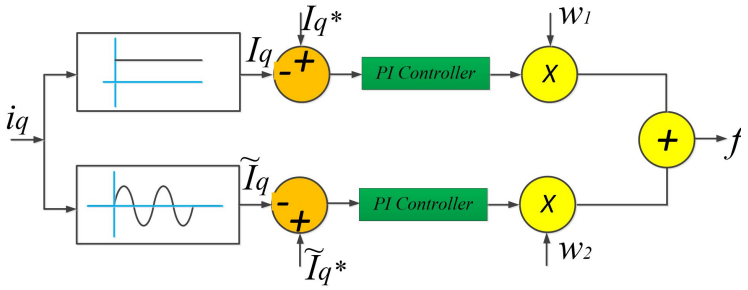

Figure 2. Front-end converter control structure.

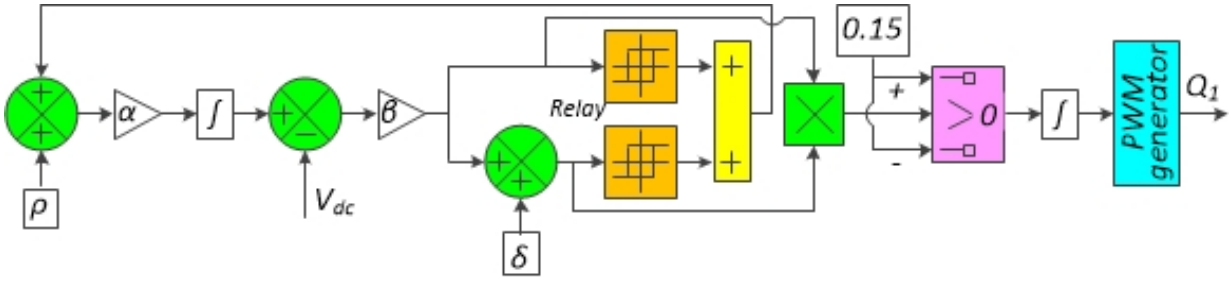

Figure 3. Sliding mode controller for PV interface DC-DC boost converter.

3. Control structure

3.1. Front end converter control

The q-axis component of motor current was obtained from sensed phase currents. The low pass filter and ripple extractor were employed to filter average value and ripple content in the q-axis component of grid current respectively as shown in Fig. 2. These components were then verified for limit of regulation. Otherwise, PI regulator is activated to limit the output frequency command. The error in reference and current value of respective q-axis current components were multiplied by respective weights and were summed. This weighted sum function of q-axis component of source current components was fed to PI regulator which would determine the acceleration or deceleration of frequency which when added to set frequency would determine the output frequency command. During this process, the weights of each component were user defined so that average q-axis current and q-axis ripple current were simultaneously regulated to reference levels at any given instant.

3.2. PV interface DC-DC Boost Converter with SMC

Single-phase supply is converted to DC to run a three-phase induction motor through a three-phase inverter. The output voltage of the diode rectifier is a pulsated DC, and it is needed to provide a smooth DC link voltage to the inverter to minimize the ripple factor of the induction motor. Hence, the SMC is implemented to boost the converter to generate a smooth DC output supply. The implemented SMC is shown in Fig. 3 for generating pulses to Q_1, where δ, β, ρ and α are constants chosen by the tuning method.

3.3. Sensor less Speed Estimation

It is very difficult to sense the speed under high depth where the motor is underwater. Hence, estimation of speed using mathematical equations can help design induction motor sensor-less speed controllers [30, 31]. The block diagram of speed estimation using the model reference adaptive controller (MRAC) of IM is

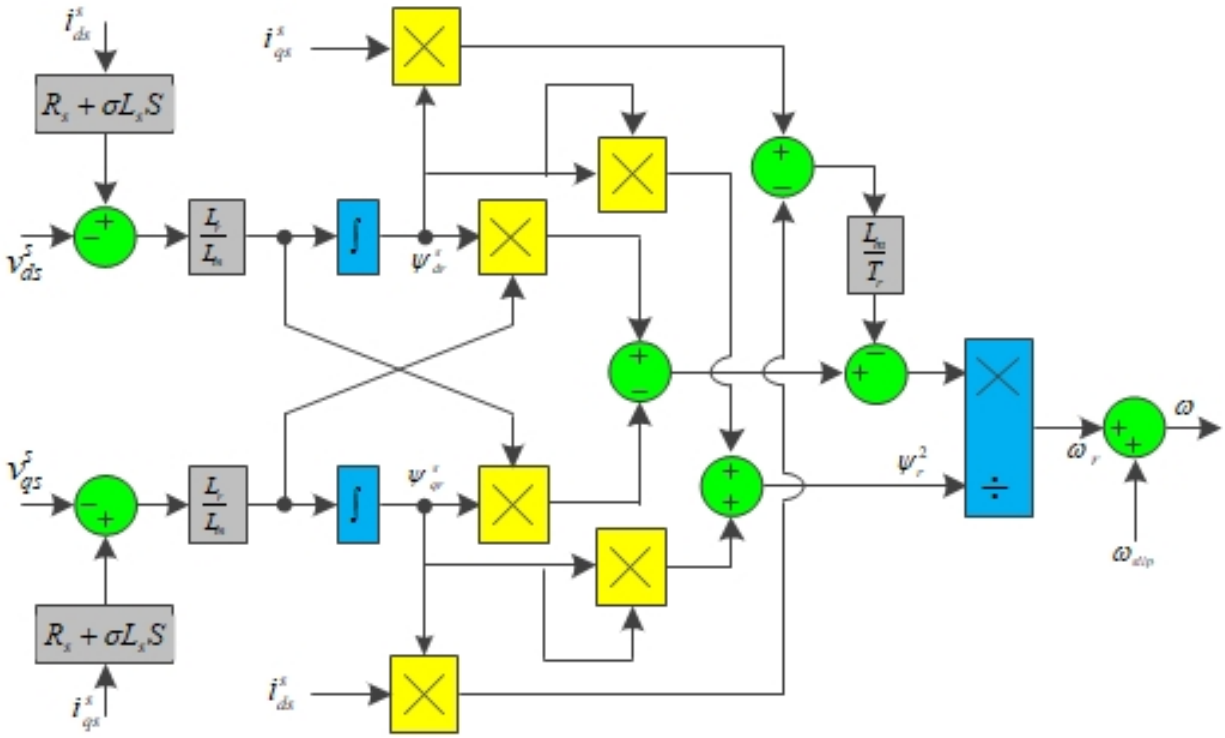

Figure 4. Speed estimation by MRAC.

shown in Fig. 4. The output of the inverter (i.e., input of IM) depends on both v_{dc} and pulses generated by the PWM generator. Hence, inverter voltages can obtain with the help of mathematical expressions [32, 33]. Therefore, physical voltage sensors are not required to sense the input voltage of IM. It makes the system more cost-effective.

The following equations (5 - 14) can estimate the speed:

$$v^s_{ds} = i^s_{ds} R_s + L_{ls} \frac{d}{dt} i^s_{ds} + \frac{d}{dt} \psi^s_{dm} \ , \tag{5}$$

$$v^s_{ds} = \frac{L_m}{L_r} \frac{d}{dt} (\psi^s_{dr}) + (R_s + \sigma L_{ls} S) i^s_{ds} \ , \tag{6}$$

where $\sigma = 1 - \frac{L_m^2}{L_m L_r}$.

$$\frac{d}{dt} (\psi^s_{dr}) = \frac{L_r}{L_m} v^s_{ds} - \frac{L_r}{L_m} (R_s + \sigma L_{ls} S) i^s_{ds} \ , \tag{7}$$

similarly,

$$\frac{d}{dt} (\psi^s_{qr}) = \frac{L_r}{L_m} v^s_{qs} - \frac{L_r}{L_m} (R_s + \sigma L_{ls} S) i^s_{qs} \ , \tag{8}$$

$$\frac{d}{dt} (\psi^s_{dr}) = \frac{L_m}{T_r} i^s_{ds} - \omega_s \psi^s_{qr} - \frac{1}{T_r} q^s_{dr} \ , \tag{9}$$

$$\frac{d}{dt} (\psi^s_{qr}) = \frac{L_m}{T_r} i^s_{qs} + \omega_s \psi^s_{dr} - \frac{1}{T_r} q^s_{qr} \ , \tag{10}$$

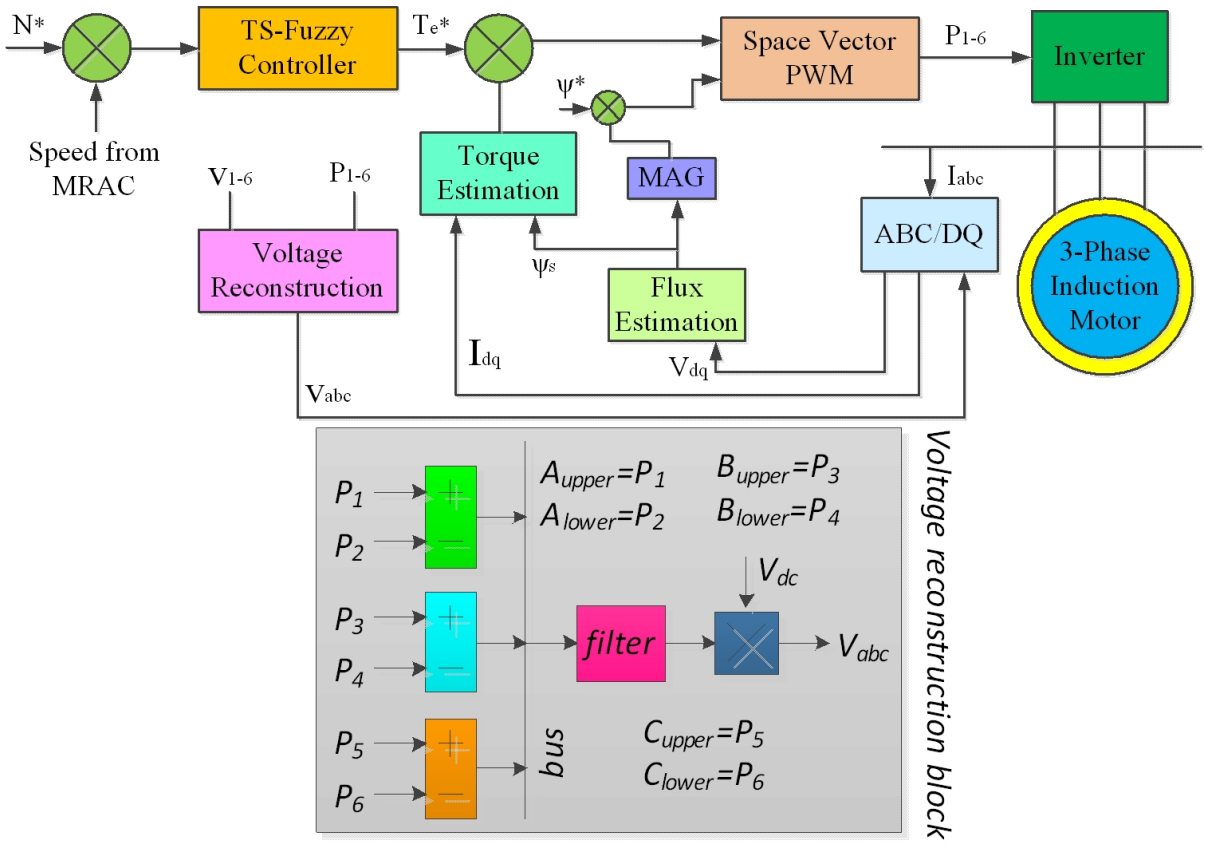

Figure 5. TS-Fuzzy-based DTC of induction motor.

where $T_r = L_r/R_r$. Moreover, angle of rotor can be estimated by,

$$\theta_e = Tan^{-1}\left(\frac{\psi^s_{qr}}{\psi^s_{dr}}\right) \quad , \tag{11}$$

hence, the rotor speed is calculated by,

$$\omega_r = \frac{d}{dt}\theta_e = \frac{1}{\psi_r^2}\left[\left(\psi^s_{dr}\frac{d}{dt}\psi^s_{qr} - \psi^s_{qr}\frac{d}{dt}\psi^s_{dr}\right) - \frac{L_m}{T_r}\left(\psi^s_{dr}i^s_{qs} - \psi^s_{qr}i^s_{ds}\right)\right] \quad . \tag{12}$$

Slip speed is given by,

$$\omega_{slip} = \frac{1+\sigma T_r S}{T_r(\psi_{ds} - \sigma L_s i_{ds})} \quad , \tag{13}$$

hence, the speed of IM (for indirect vector control) can be estimated by

$$\omega = \omega_{slip} + \omega_r \quad . \tag{14}$$

3.4. TS-Fuzzy based Direct Torque Control

The schematic of TS-Fuzzy based direct torque control of VSI fed induction motor is shown in Fig. 5. The sensed DC link voltage and gating signals construct the motor phase voltages. The scheme of generating phase voltages from DC link voltage and gating pulses was also shown in Fig. 5. The gating signals were

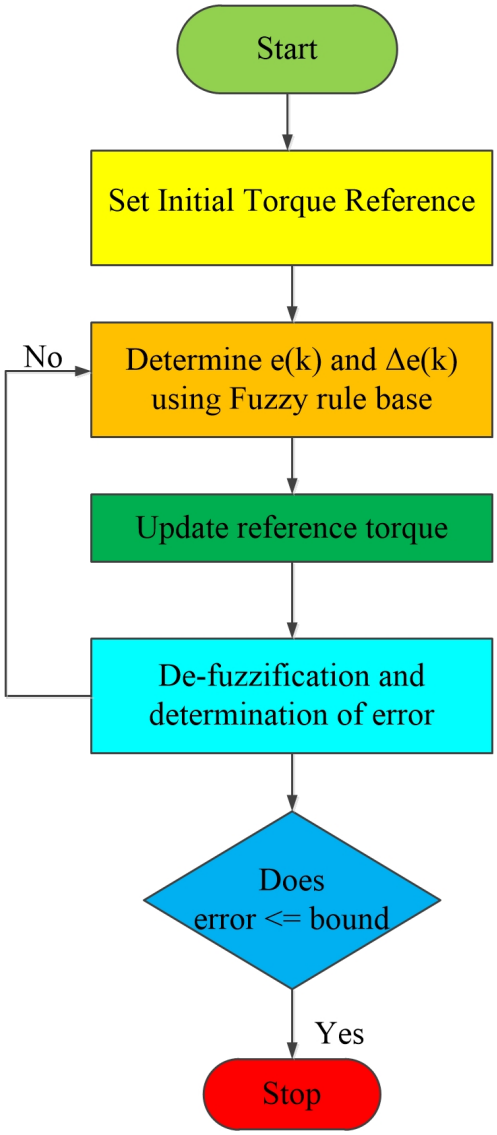

Figure 6. Flowchart for TS-Fuzzy control implementation.

multiplexed and logically added to obtain templates for each phase. A low pass filter with a cutoff frequency just above the line frequency provided unit magnitude sine wave templates of each phase which were multiplied by DC link voltage to construct phase voltages of the motor. The phase currents and obtained phase voltages were then transformed into d - q coordinates. The phase voltages in the d - q system were utilized to estimate air gap flux. The phase currents in the d - q system and flux angle generated from the flux estimator were fed to the torque estimator. The error generated from reference speed and estimated speed from model reference adaptive control (MRAC) was fed as input to the TS-Fuzzy controller which generates reference torque. The error in torque and flux map to respective instantaneous voltage vector to be generated by space vector pulse width modulator.

The flow chart for implementing FLC is shown in Fig. 6. Initial guess of torque reference was set to 0.5 pu. The TS-Fuzzy controller was discussed in this section. The input variables for designing the TS-Fuzzy controller variations x_i and its derivative $\dot{x_i}$ in current and voltage as shown in Fig. 7. Inputs fuzzification was realized using the membership function [21] as shown in Fig. 7.

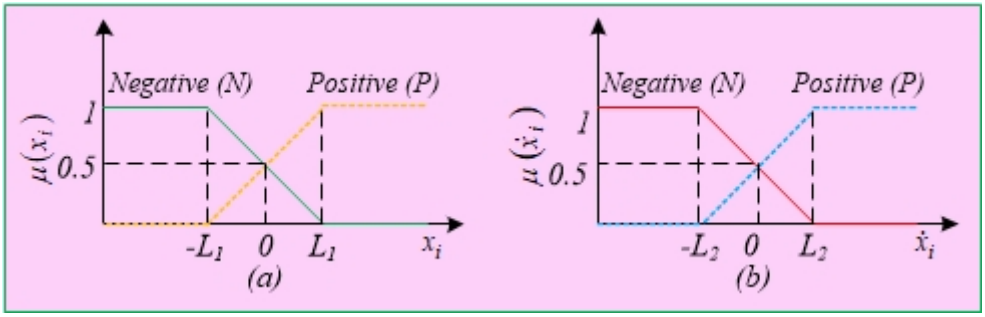

Figure 7. TS-Fuzzy membership functions.

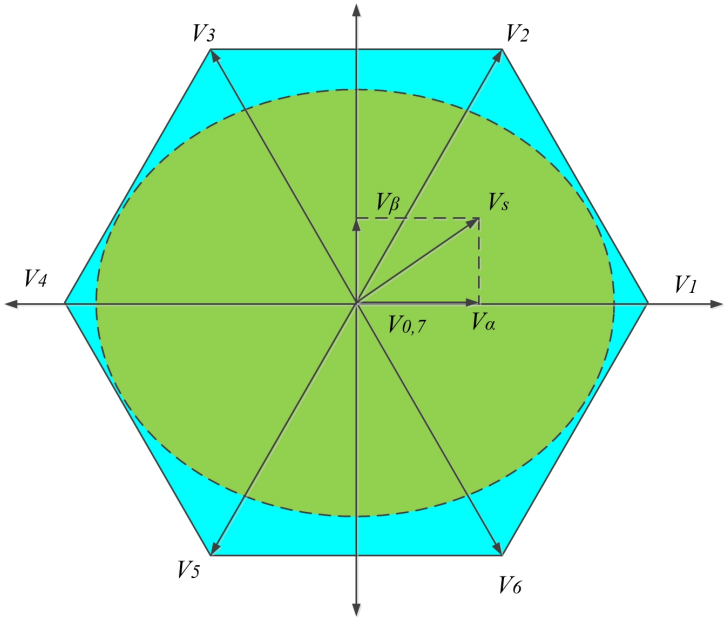

$V_1 \sim [0 < \Theta \leq 60] = (A_{upper}, B_{lower}, C_{lower})$

$V_2 \sim [60 < \Theta \leq 120] = (A_{upper}, B_{upper}, C_{lower})$

$V_3 \sim [120 < \Theta \leq 180] = (A_{lower}, B_{upper}, C_{lower})$

$V_4 \sim [180 < \Theta \leq 240] = (A_{lower}, B_{upper}, C_{upper})$

$V_5 \sim [240 < \Theta \leq 300] = (A_{lower}, B_{lower}, C_{upper})$

$V_6 \sim [300 < \Theta \leq 360] = (A_{upper}, B_{lower}, C_{upper})$

$V_{10,7} \sim [Null]$

Figure 8. VSI current control.

The MFs for and signals are stated in,

$$\mu_p(x_i) = \begin{cases} 0 & x_i < L_1 \\ \frac{x_i + L_1}{2L_1} & -L_1 \leqslant x_i \leq L_1 \\ 1 & x_i > L_1 \end{cases}$$
$$\mu_N(x_i) = \begin{cases} 0 & x_i < L_1 \\ \frac{-x_i + L_1}{2L_1} & -L_1 \leqslant x_i \leq L_1 \\ 1 & x_i > L_1 \end{cases}, \quad (15)$$

$$\mu_p(\dot{x_i}) = \begin{cases} 0 & \dot{x_i} < L_1 \\ \frac{\dot{x_i} + L_1}{2L_1} & -L_1 \leqslant \dot{x_i} \leq L_1 \\ 1 & \dot{x_i} > L_1 \end{cases}$$
$$\mu_N(\dot{x_i}) = \begin{cases} 0 & \dot{x_i} < L_1 \\ \frac{-\dot{x_i} + L_1}{2L_1} & -L_1 \leqslant \dot{x_i} \leq L_1 \\ 1 & \dot{x_i} > L_1 \end{cases}, \quad (16)$$

and the rules corresponding to the TS-Fuzzy controller are given in Table 1.

Table 1. The TS-Fuzzy controller rules.

Rule	$x_i(k)$	$\dot{xi}(k)$	Value
Rule 1	N	N	$Z_1 = a_1 x_i(k) + a_2 \dot{x_i}(k)$
Rule 2	N	P	$Z_2 = a_3 Z_1$
Rule 3	P	N	$Z_3 = a_4 Z_1$
Rule 4	$x_i(k)$	$\dot{xi}(k)$	Value

In Table 1, the calculated output of the TS-Fuzzy operation is characterized by Z_1, Z_2, Z_3, and Z_4. k denotes the sampling. instant. a_1, a_2, a_3, a_4, and a_5 designate the fuzzy constants, tuned by a tuning process that diverges from one controller to another. A generalized defuzzifier is exploited to return the controller's output Y as expressed by,

$$Y = \frac{Z_1 F_1 + Z_2 F_2 + Z_3 F_3 + Z_4 F_4}{Z_1 + Z_2 + Z_3 + Z_4} \quad , \tag{17}$$

where $F_1 =$ Minimum $\{\mu_p \dot{x_i}, \mu_p x_i\}$ and $F_2 =$ Minimum $\{\mu_N \dot{x_i}, \mu_N x_i\}$. TS-Fuzzy is implemented to generate reference torque by comparing motor speed to its reference speed [30]. Hence the output Y is dynamically adjusted to improve the performance and stability during system dynamics. In this proposed system, a smooth reference torque signal can help minimize ripples in generated electromagnetic torque from the induction motor. The membership function used for the positive set and negative set is determined using equations (15) and (16).

4. Simulation Results

The switching frequency of the inverter can be limited by adjusting the large hysteresis band and the range of that frequency is determined thermal limit of power devices. In lower-speed regions, the performance of the system will decrease because the hysteresis bands are adjusted to cope with the worst conditions. While controlling the torque, the hysteresis controller is set to change the elapsing time from the lower limit to the upper limit proportional to operating conditions. The model diagram of TS-Fuzzy-based DTC of induction motor is shown in Fig. 5. The phase reconstruction block was also implemented to obtain three-phase voltage without measuring the voltage at the output of the inverter. It can help to decrease the number of voltage sensors; which results in cost reduction which is represented in Fig. 6. The simulation parameters of the proposed system are given in Table 2.

Table 2. Simulation parameters for drive.

Parameter	Value
Rated power	8 kW
DC bus voltage	300 V
AC source specifications	230 V, 50 Hz
Maximum line current at AC source terminals	40 A
Induction motor rated line voltage	230 V
Power rating of induction motor	7.5 HP
Rated speed of induction motor	3450 rpm
Maximum phase current	20 A
Maximum ratings of power switches	IGBT: 300 V, 100 A
Maximum ratings of power diodes	300 V, 100 A
TS-Fuzzy Parameters	Error bound: 0.01, Membership Function: Triangular

4.1. Change in load torque

Initially, the motor has been operated at a nominal load torque of 5Nm from 0s to 1.5s and the load torque changes from 1.5s. As a result, the battery will supply the required power to the motor, for which the battery's charge gets reduced. The electromagnetic torque required to drive the load torque without changing the vehicle's speed or under a steady state can be achieved through vector control. The torque and speed of the vehicle during this scenario have been graphically represented in Fig. 9 and Fig. 10, respectively. It can be noticed from the graph given in Fig. 10 that with a significant torque increment in the motor's load torque, the vehicle's speed remains the same at stead-state. But, the motor runs at its reference speed during the change of toque scenario due to the presence of vector control in the system. However, while overcoming the electromagnetic torque over the load torque, it has been noticed that the rate of the vehicle decreased during the transient period. Fig. 11 represents the battery power curve from which it can be observed that the battery power is in negative value that indicates charging mode. The power increases to a positive value from time at 1.5s, indicating discharge mode due to the motor's start in the vehicle.

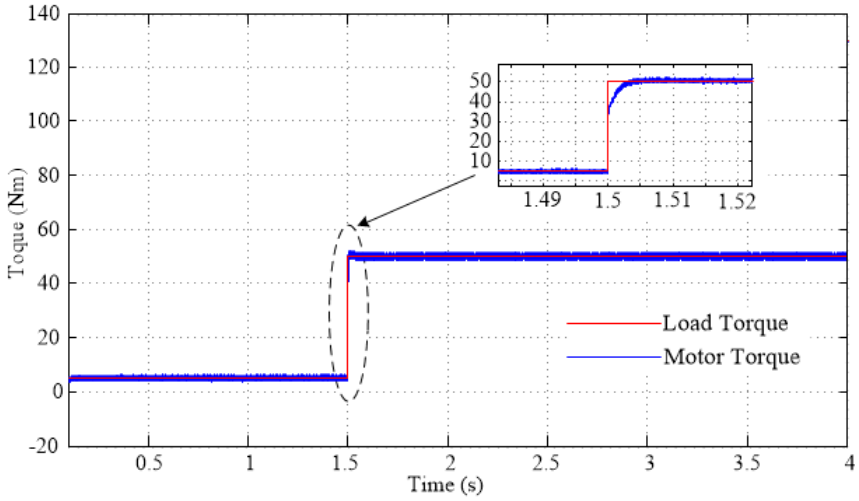

Figure 9. Load and electromagnetic torque generated by drive.

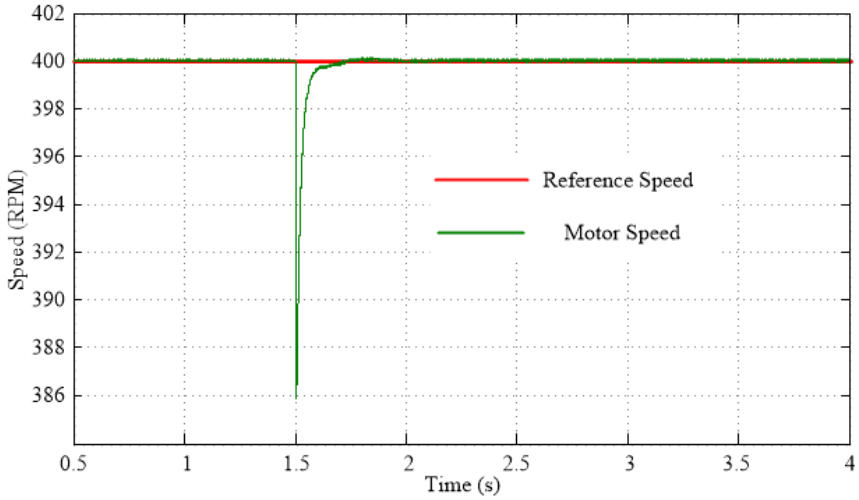

Figure 10. Response of speed under increasing load torque.

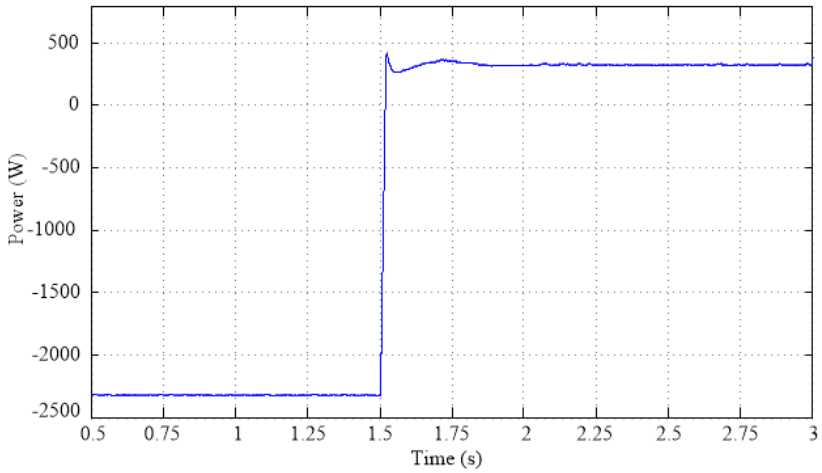

Figure 11. Response of battery under the change in load torque scenario.

4.2. Change in vehicle speed

In Electric Vehicle (EV), the speed of the vehicles rapidly changes depending on various factors, such as road conditions, traffic, etc., that change the speed of the motor. Hence, the rapid fluctuation of motor speed and the effect on the system has been studied in this case. The reference speed of the vehicle has been increased from 40kmph (320RPM for motor) to a new speed of 50kmph (400RPM for motor) at 4s time. As mentioned previously, the motor's speed will remain maintained due to the presence of vector control in the system. Fig. 12 represents the response to the speed of the motor, and it can be seen that there is an increase in the electromagnetic torque at the transient due to the increase in the speed of the motor. However, the torque generated by the motor will always follow the reference torque, which will remain unchangeable, as shown in Fig. 13. The dc-link voltage response of the converter has been depicted in Fig. 14 shows disturbances due to sudden rise and fall of the voltage rating caused by the sudden change in the motor speed. Also, there is a small spike in electromagnetic torque generated by drive due to the increase in reference speed. The torque gets stable once the speed of the motor reaches its reference value.

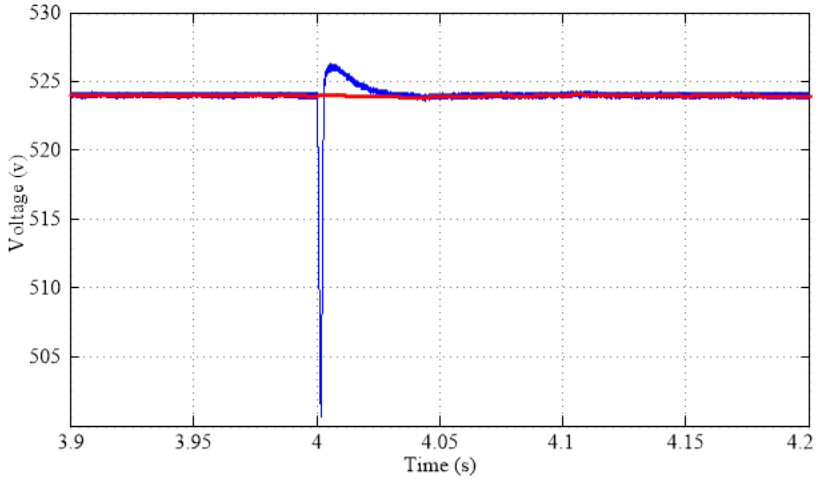

Figure 12. DC link regulation for speed change.

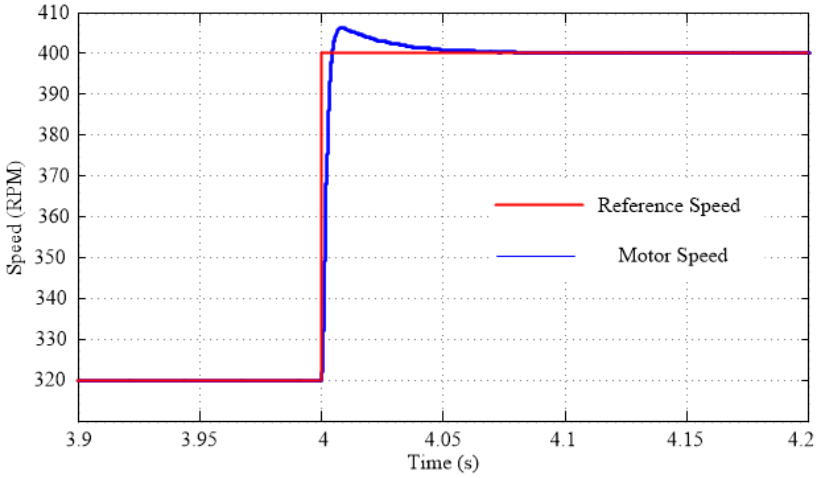

Figure 13. Speed response of the motor.

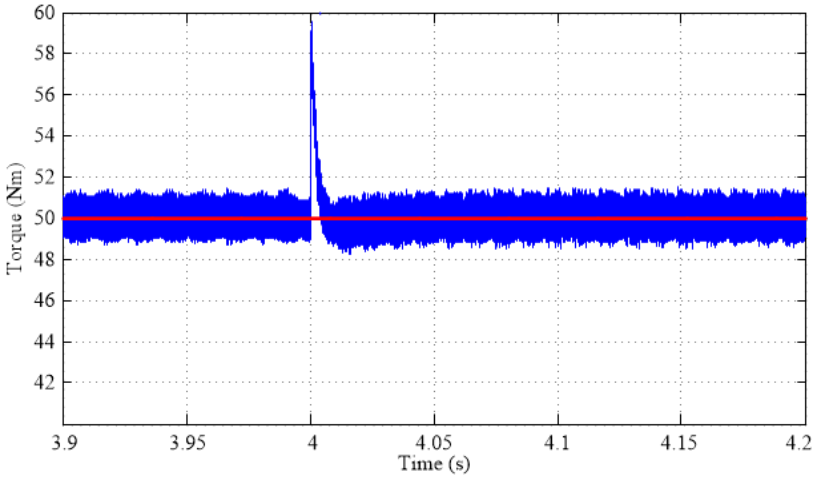

Figure 14. Torque response or change in speed.

4.3. Reverse Driving Mode of the Vehicle

In EV, the reverse operation has been mainly performed by changing the operation of the motor from forward motoring mode to reverse motoring mode, which is achieved by automatically interchanging the pulses of the converter by the vector control method. Considering at time t=4s, the vehicle goes for reverse mode at a speed of 10kmph (80 RPM of the motor), the reverse motoring mode has been achieved by changing the value of reference speed from 80RPM to -80RPM which is performed by the vector control mode as shown in Fig. 15. The sudden change in the direction of movement of the motor has caused a fluctuation in the dc-link voltage for a short period and maintained constant later on to the reference value that can be observed by visualizing the graph given in Fig. 16. The electromagnetic torque decreases suddenly due to reversal mode of the motor which is then maintained to its reference value at steady-state as shown in Fig. 17. Also, it has been noticed that the change in the motor speed and its direction has caused a minor disturbance in the dc-link voltage. Hence from the above investigation, it has been found that the proposed DTC-based controller drive for EV performed well during both steady-state and transient-state conditions.

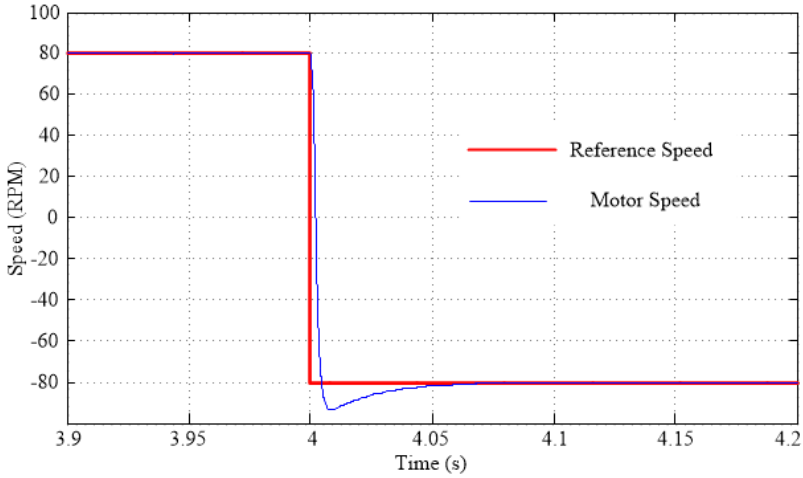

Figure 15. Reference and motor speed in the reverse direction.

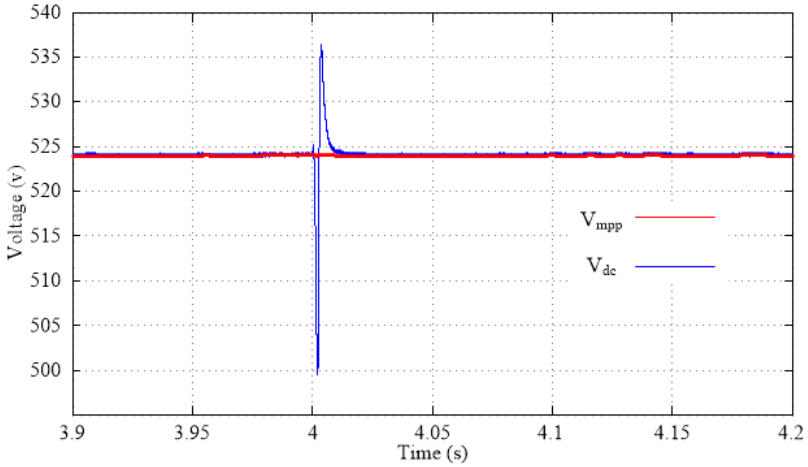

Figure 16. DC link voltage due to change in the direction of rotation of the motor.

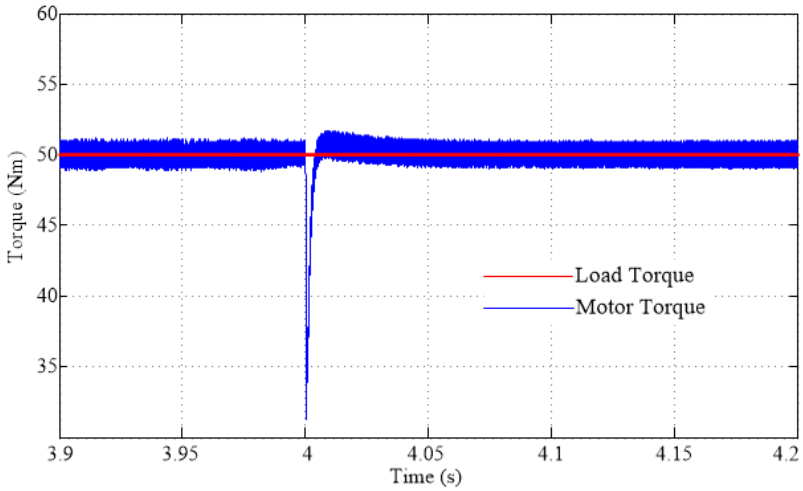

Figure 17. Response of load torque and electromagnetic torque under the change in speed.

5. Conclusion

The closed loop operation for agricultural pump drive with proposed topology and control is discussed. The model for pump load and sizing of the motor is presented. The MRAC for speed estimation is presented. TS-Fuzzy logic based direct torque control structure employed for closed-loop speed control is discussed. The frequency regulation for minimizing input current ripple was observed. DC bus was regulated with only 6.25 percent ripple. Maximum available power from PV source is extracted which accounted to 42 percent of total load requirement. A good transient response in all cases was obtained. Achieved maximum overshoot of 5 rpm and torque spike (or dip) of 5 N-m for step change in speed. Also, transient time of 0.2 sec for sudden increment or decrement in load torque by 50 percent was obtained. Thus, a reliable drive for rural agricultural needs was developed.

Acknowledgments

Funding: This research received no external funding.

Author contributions: Conceptualization, S.V.R.R, R.M, M.K.K, C.R.R and T.V.S; Methodology, D.R.K and B.N.R; Software, M.K.K; Validation, C.R.R, T.V.S and D.R.K; Formal Analysis, M.K.K; Investigation, R.M; Resources, R.M; Data Curation, M.K.K; Writing – Original Draft Preparation, R.M, S.V.R.R; Writing–Review & Editing, D.R.K, S.V.R.R; Visualization, T.V.S, C.R.R; Supervision, M.K.K, C.R.R; Project Administration, M.K.K, S.V.R.R; Funding Acquisition, M.K.K, C.R.R.

Disclosure statement: The authors declare no conflict of interest.

References

[1] Ashok Kumar Kolluru, Malligunta Kiran Kumar, S Ravi Teja, Rami Reddy, Mohammed Alqahtani, and Muhammad Khalid. Novel controller for pv fed water pumping optimization system driven by 8/6 pole srm with asymmetrical converter. *Frontiers in Energy Research*, 11:1205704, 2023.

[2] B Nagi Reddy, K Sarada, M Bharathi, Y Anil Kumar, Ch Rami Reddy, and B Srikanth Goud. Five level h-bridge configuration based microgrid with sugeno fuzzy controller for new energy generation from renewable systems. *Transactions on Energy Systems and Engineering Applications*, 4(2):1–14, 2023.

[3] Saurabh Shukla and Bhim Singh. Reduced-sensor-based pv array-fed direct torque control induction motor drive for water pumping. *IEEE Transactions on Power Electronics*, 34(6):5400–5415, 2018.

[4] Arunachalam Sivakumar, Muthamizhan Thiyagarajan, and Karthick Kanagarathinam. Mitigation of supply current harmonics in fuzzy-logic based 3-phase induction motor. *International Journal of Power Electronics and Drive Systems*, 14(1):266, 2023.

[5] Khusro Khan, Saurabh Shukla, and Bhim Singh. Single-phase grid-fed variable frequency high-efficiency induction motor drive for fan applications. *IET Energy Systems Integration*, 4(1):54–71, 2022.

[6] Mahesh M Swamy, Anupama Balakrishnan, and Joshua Collins. Getting the most from a variable frequency drive: The optimal way to improve lifetime and reliability. *IEEE Industry Applications Magazine*, 22(6):57–65, 2016.

[7] Mohammed Ali Khan, Ahteshamul Haque, Varaha Satya Bharath Kurukuru, and Frede Blaabjerg. Optimizing the performance of single-phase photovoltaic inverter using wavelet-fuzzy controller. *e-Prime-Advances in Electrical Engineering, Electronics and Energy*, 3:100093, 2023.

[8] E Ramakrishna and Vinay Kumar. Anfis based grid connected solar pv based water pumping using bldc motor drive. *Industrial Engineering Journal*, 52:2293–98, 2023.

[9] Senthilnathan Rajendran, Vigneysh Thangavel, Narayanan Krishnan, and Natarajan Prabaharan. Dc link voltage enhancement in dc microgrid using pv based high gain converter with cascaded fuzzy logic controller. *Energies*, 16(9):3928, 2023.

[10] François Yonga, Colince Welba, Theodore Louossi, and Noël Djongyang. A new control approach of a three-phase inverter two levels. *Open Journal of Energy Efficiency*, 11(3):55–70, 2022.

[11] Rajan Kumar and Bhim Singh. Single stage solar pv fed brushless dc motor driven water pump. *IEEE Journal of Emerging and Selected Topics in Power Electronics*, 5(3):1377–1385, 2017.

[12] S Sashidhar, V Guru Prasad Reddy, and BG Fernandes. A single-stage sensorless control of a pv-based bore-well submersible bldc motor. *IEEE Journal of Emerging and Selected Topics in Power Electronics*, 7(2):1173–1180, 2018.

[13] Prasoon Chandran Mavila and PP Rajeevan. A five-level torque controller based dtc scheme for open-end winding five-phase im drives with single dc source and auxiliary plane harmonic elimination. *IEEE Transactions on Industry Applications*, 58(2):2063–2074, 2022.

[14] Chandra Sekhar et al. Implementation of zero current switch turn-on based buck-boost-buck type rectifier for low power applications. *International Journal of Electronics*, 106(8):1164–1183, 2019.

[15] Ashok Kumar Kolluru and Kiran Kumar Malligunta. Closed-loop speed control of switched reluctance motor drive fed from novel converter with reduced number of switches. *International Journal of Power Electronics and Drive Systems*, 11(1):189, 2020.

[16] L Sri Sivani, L Nagi Reddy, BK SubbaRao, and A Pandian. A new single switch ac/dc converter with extended voltage conversion ratio for smps applications. *Int. Journal of Innovative Technology and Exploring Engineering*, 8(3):68–72, 2019.

[17] Pazhanimuthu Cholamuthu, Baranilingesan Irusappan, Suresh Kalichikadu Paramasivam, Senthil Kumar Ramu, Suresh Muthusamy, Hitesh Panchal, Ramakrishna SS Nuvvula, Polamarasetty P Kumar, Baseem Khan, et al. A grid-connected solar pv/wind turbine based hybrid energy system using anfis controller for hybrid series active power filter to improve the power quality. *International Transactions on Electrical Energy Systems*, 2022:1–14, 2022.

[18] Mudundi Rekha and Kiran Kumar Malligunta. Variable frequency drive optimization using torque ripple control and self-tuning pi controller with pso. *International Journal of Electrical and Computer Engineering*, 9(2):802, 2019.

[19] Chong Li et al. Comparative performance analysis of grid-connected pv power systems with different pv technologies in the hot summer and cold winter zone. *International Journal of Photoenergy*, 2018:1–10, 2018.

[20] H Maammeur, A Hamidat, L Loukarfi, M Missoum, K Abdeladim, and T Nacer. Performance investigation of grid-connected pv systems for family farms: case study of north-west of algeria. *Renewable and Sustainable Energy Reviews*, 78:1208–1220, 2017.

[21] Ahmed K Abdelsalam, Mahmoud I Masoud, Mostafa S Hamad, and Barry W Williams. Modified indirect vector control technique for current-source induction motor drive. *IEEE Transactions on Industry Applications*, 48(6):2433–2442, 2012.

[22] Theodore Louossi, Fabrice Kwefeu Mbakop, Abdouramani Dadje, Noel Djongyang, et al. Modeling of an electrical energy switching system in multisource power plants: The case of grid connected photovoltaic and wind power systems. *Journal of Renewable Energy*, 2022:1–15, 2022.

[23] P Satish Kumar, RPS Chandrasena, V Ramu, GN Srinivas, and K Victor Sam Moses Babu. Energy management system for small scale hybrid wind solar battery based microgrid. *IEEE access*, 8:8336–8345, 2020.

[24] Atallah Ouai, Lakhdar Mokrani, Mohamed Machmoum, and Azeddine Houari. Control and energy management of a large scale grid-connected pv system for power quality improvement. *Solar Energy*, 171:893–906, 2018.

[25] Kai Cui, Chenchen Wang, Minglei Zhou, and Shengquan Sun. Comprehensive investigation of space-vector pwm including novel switching sequences for dual three-phase motor drives. *IEEE Transactions on Transportation Electrification*, 9(1):1350–1362, 2022.

[26] Mahesh M Swamy, Joshua Collins, and Anupama Balakrishnan. An optimal solution for operating a three-phase variable frequency drive from a single-phase ac source. In *2014 IEEE Energy Conversion Congress and Exposition (ECCE)*, pages 1699–1706. IEEE, 2014.

[27] Yaser Nabeel Ibrahem Alothman, Wisam Essmat Abdul-Lateef, and Sabah Abdul-Hassan Gitaffa. Using sensorless direct torque with fuzzy proportional-integral controller to control three phase induction motor. *Bulletin of Electrical Engineering and Informatics*, 12(2):738–748, 2023.

[28] Tayyaba Nosheen, Ahsan Ali, Muhammad Umar Chaudhry, Dmitry Nazarenko, Inam ul Hasan Shaikh, Vadim Bolshev, Muhammad Munwar Iqbal, Sohail Khalid, and Vladimir Panchenko. A fractional order controller for sensorless speed control of an induction motor. *Energies*, 16(4):1901, 2023.

[29] S Chandrasekaran, S Durairaj, and S Padmavathi. A performance evaluation of a fuzzy logic controller-based photovoltaic-fed multi-level inverter for a three-phase induction motor. *Journal of the Franklin Institute*, 358(15):7394–7412, 2021.

[30] Ahmed Jadaan Ali, Ziyad Farej, and Nashwan Sultan. Performance evaluation of a hybrid fuzzy logic controller based on genetic algorithm for three phase induction motor drive. *International Journal of Power Electronics and Drive Systems*, 10(1):117, 2019.

[31] Abolfazl Mehbodniya, Parmod Kumar, Xie Changqing, Julian L Webber, Udit Mamodiya, Awal Halifa, Chennupalli Srinivasulu, et al. Hybrid optimization approach for energy control in electric vehicle controller for regulation of three-phase induction motors. *Mathematical Problems in Engineering*, 2022:1–13, 2022.

[32] Lelisa Wogi, Tadele Ayana, Marcin Morawiec, and Andrzej Jąderko. A comparative study of fuzzy smc with adaptive fuzzy pid for sensorless speed control of six-phase induction motor. *Energies*, 15(21):8183, 2022.

[33] CN Bhende, S Mishra, and SK Jain. Ts-fuzzy-controlled active power filter for load compensation. *IEEE transactions on power delivery*, 21(3):1459–1465, 2006.